

# Non-standard Charged Current Interactions: beta decays versus the LHC

Vincenzo Cirigliano<sup>1</sup>, Martín González-Alonso<sup>2</sup>, Michael L. Graesser<sup>1</sup>

<sup>1</sup>) Theoretical Division, Los Alamos National Laboratory, Los Alamos, NM 87545, USA

<sup>2</sup>) Department of Physics, University of Wisconsin-Madison,  
1150 University Ave., Madison, WI, 53706, USA

## Abstract

We discuss low-energy and collider constraints on the effective couplings characterizing non-standard charged current interactions. A direct comparison of low-energy and LHC probes can be performed within an effective theory framework, when the new physics mediating these interactions originates in the multi-TeV scale. We find that for the effective couplings involving right-handed neutrinos the LHC bounds from  $pp \rightarrow e + MET + X$  are at the (sub)percent level, already stronger than those from  $\beta$  decays. For operators involving left-handed neutrinos, the (axial-)vector and pseudo-scalar effective couplings are best probed at low energy, while scalar and tensor couplings are currently probed at the same level by beta decays and the LHC channels  $pp \rightarrow e + MET + X$  and, by using SU(2) gauge invariance,  $pp \rightarrow e^+e^- + X$ . Future beta decay experiments at the 0.1% level or better will compete in sensitivity with higher statistics and higher energy data from the LHC.

# 1 Introduction

Beta decays have played a central role in determining the  $V - A$  structure of charged current (CC) weak interactions and in shaping what we now call the Standard Model (SM) [1, 2]. Nowadays, precision beta-decay measurements with neutrons, nuclei, and mesons [2] can be used to probe the existence of non-standard CC interactions that would induce effective violations of Cabibbo universality and lepton universality, and distinctive non-V-A signatures in the decay spectra and correlations.

Low-energy CC processes are sensitive to many classes of SM extensions and various mechanisms (tree level mediation by novel vector or scalar bosons, vertex corrections, box diagrams, etc) [3]. For example, for recent discussions of supersymmetric contributions see Refs. [4, 5]. More generally, the new physics reach of low-energy beta decays can be studied in a model-independent way within an effective field theory (EFT) setup, in which the dynamical effects of new heavy BSM degrees of freedom are parameterized by local operators, built with SM fields, and of dimension higher than four. In this sense, 0.1% level (or better) beta decay measurements provide “broad band” probe of BSM interactions, enforcing powerful low-energy boundary conditions on virtually any SM extension at the TeV scale, currently probed at the Large Hadron Collider (LHC).

In this letter we wish to compare the new physics reach of low-energy beta decay measurements and  $pp$  collisions at the LHC in constraining non-standard CC interactions. Such a comparison is in principle model-dependent, since it requires knowing the detailed dynamics of the SM extension. However, if the particles that mediate the new interactions are above threshold for production at colliders, then the EFT analysis is valid at collider energies and a direct comparison of low-energy and collider constraints can be performed.

Working in the latter scenario, we present in Section 2 the complete set of  $SU(2) \times U(1)$ -invariant operators that contribute to CC processes, involving the SM fields and right-handed singlet neutrinos. We then discuss the evolution of the effective Lagrangian down to hadronic scales and the matching to a nucleon-level effective theory. In Section 3 we summarize the current bounds from low-energy and briefly discuss the reach of future beta decay experiments. In Section 4 we compute the bounds on non-standard interactions arising from the processes  $pp \rightarrow e + MET + X$  and  $pp \rightarrow e^+e^- + X$  at the LHC, and show that the combination of low-energy and LHC searches provides a much stronger set of constraints on non-standard CC interactions. We present our final comments in Section 5.

## 2 EFT Analysis of Charged Current Processes

### 2.1 Weak-scale Operator Basis

The building blocks to construct gauge-invariant local operators are the gauge fields  $G_\mu^A$ ,  $W_\mu^a$ ,  $B_\mu$ , corresponding to  $SU(3) \times SU(2)_L \times U(1)_Y$ , the six fermionic gauge multiplets

(now including a singlet right-handed neutrino state),

$$q^i = \begin{pmatrix} u_L^i \\ d_L^i \end{pmatrix} \quad u^i = u_R^i \quad d^i = d_R^i \quad l^i = \begin{pmatrix} \nu_L^i \\ e_L^i \end{pmatrix} \quad e^i = e_R^i \quad \nu^i = \nu_R^i, \quad (2.1)$$

the Higgs doublet  $\varphi$

$$\varphi = \begin{pmatrix} \varphi^+ \\ \varphi^0 \end{pmatrix}, \quad (2.2)$$

and the covariant derivative

$$D_\mu = I \partial_\mu - ig_s \frac{\lambda^A}{2} G_\mu^A - ig \frac{\sigma^a}{2} W_\mu^a - ig' Y B_\mu. \quad (2.3)$$

In the above expression  $\lambda^A$  are the  $SU(3)$  Gell-Mann matrices,  $\sigma^a$  are the  $SU(2)$  Pauli matrices,  $g_s, g, g'$  are the gauge couplings and  $Y$  is the hypercharge of a given multiplet.

The minimal and complete set of dimension-six operators contributing to low-energy semi-leptonic charged current processes can be divided into two groups (operators involving the singlet  $\nu$  are displayed on the right columns below).

Four-fermion operators:

$$O_{lq}^{(3)} = (\bar{l} \gamma^\mu \sigma^a l) (\bar{q} \gamma_\mu \sigma^a q) \quad O_{e\nu ud} = (\bar{e} \gamma^\mu \nu) (\bar{u} \gamma_\mu d) + \text{h.c.} \quad (2.4a)$$

$$O_{qde} = (\bar{l} e) (\bar{d} q) + \text{h.c.} \quad O_{qu\nu} = (\bar{l} \nu) (\bar{u} q) + \text{h.c.} \quad (2.4b)$$

$$O_{lq} = (\bar{l}_a e) \epsilon^{ab} (\bar{q}_b u) + \text{h.c.} \quad O'_{lq} = (\bar{l}_a \nu) \epsilon^{ab} (\bar{q}_b d) + \text{h.c.} \quad (2.4c)$$

$$O_{lq}^t = (\bar{l}_a \sigma^{\mu\nu} e) \epsilon^{ab} (\bar{q}_b \sigma_{\mu\nu} u) + \text{h.c.} \quad O_{lq}^{t'} = (\bar{l}_a \sigma^{\mu\nu} \nu) \epsilon^{ab} (\bar{q}_b \sigma_{\mu\nu} d) + \text{h.c.} \quad (2.4d)$$

Vertex corrections:

$$O_{\varphi\varphi} = i(\varphi^T \epsilon D_\mu \varphi) (\bar{u} \gamma^\mu d) + \text{h.c.} \quad O'_{\varphi\varphi} = i(\varphi^T \epsilon D_\mu \varphi) (\bar{\nu} \gamma^\mu e) + \text{h.c.} \quad (2.5a)$$

$$O_{\varphi q}^{(3)} = i(\varphi^\dagger D^\mu \sigma^a \varphi) (\bar{q} \gamma_\mu \sigma^a q) + \text{h.c.} \quad (2.5b)$$

$$O_{\varphi l}^{(3)} = i(\varphi^\dagger D^\mu \sigma^a \varphi) (\bar{l} \gamma_\mu \sigma^a l) + \text{h.c.} \quad (2.5c)$$

Denoting with  $\Lambda_i$  the effective dimensionful coupling associated with the operator  $O_i$ , we can write the effective Lagrangian as

$$\mathcal{L}^{(\text{eff})} = \mathcal{L}_{\text{SM}} + \sum_i \frac{1}{\Lambda_i^2} O_i \longrightarrow \mathcal{L}_{\text{SM}} + \frac{1}{v^2} \sum_i \hat{\alpha}_i O_i, \quad \text{with } \hat{\alpha}_i = \frac{v^2}{\Lambda_i^2}, \quad (2.6)$$

where in the last step we have set the correct dimensions by the Higgs VEV  $v = \langle \varphi^0 \rangle = (2\sqrt{2}G_F)^{-1/2}$  and defined the dimensionless new-physics couplings  $\hat{\alpha}_i$ , which in general are matrices in both quark and lepton flavor spaces.

## 2.2 Low-scale Effective Lagrangian

In this framework one can derive the low-scale  $O(1 \text{ GeV})$  effective Lagrangian for semi-leptonic transitions. It receives contributions from both  $W$ -exchange diagrams (with modified  $W$ -fermion couplings) and the four-fermion operators. This matching procedure leads to

$$\begin{aligned}
\mathcal{L}_{\text{CC}} = & -\frac{G_F^{(0)} V_{ud}}{\sqrt{2}} \left[ \left(1 + \epsilon_L\right) \bar{e} \gamma_\mu (1 - \gamma_5) \nu_\ell \cdot \bar{u} \gamma^\mu (1 - \gamma_5) d \right. \\
& + \tilde{\epsilon}_L \bar{e} \gamma_\mu (1 + \gamma_5) \nu_\ell \cdot \bar{u} \gamma^\mu (1 - \gamma_5) d \\
& + \epsilon_R \bar{e} \gamma_\mu (1 - \gamma_5) \nu_\ell \cdot \bar{u} \gamma^\mu (1 + \gamma_5) d + \tilde{\epsilon}_R \bar{e} \gamma_\mu (1 + \gamma_5) \nu_\ell \cdot \bar{u} \gamma^\mu (1 + \gamma_5) d \\
& + \epsilon_S \bar{e} (1 - \gamma_5) \nu_\ell \cdot \bar{u} d + \tilde{\epsilon}_S \bar{e} (1 + \gamma_5) \nu_\ell \cdot \bar{u} d \\
& - \epsilon_P \bar{e} (1 - \gamma_5) \nu_\ell \cdot \bar{u} \gamma_5 d - \tilde{\epsilon}_P \bar{e} (1 + \gamma_5) \nu_\ell \cdot \bar{u} \gamma_5 d \\
& \left. + \epsilon_T \bar{e} \sigma_{\mu\nu} (1 - \gamma_5) \nu_\ell \cdot \bar{u} \sigma^{\mu\nu} (1 - \gamma_5) d + \tilde{\epsilon}_T \bar{e} \sigma_{\mu\nu} (1 + \gamma_5) \nu_\ell \cdot \bar{u} \sigma^{\mu\nu} (1 + \gamma_5) d \right].
\end{aligned} \tag{2.7}$$

Here  $e, u, d$  denote the electron, up- and down-quark mass eigenfields, while  $\nu_\ell$  represents the neutrino flavor fields, with in general  $\ell \neq e$ . In what follows, we suppress lepton flavor indices. Whenever observables involving neutrinos are considered, a summation over the (unobservable) neutrino flavors is assumed. The non-standard effective couplings  $\epsilon_i$  and  $\tilde{\epsilon}_i$  are given in terms of the weak-scale couplings  $\hat{\alpha}_j$  as follows <sup>1</sup>:

$$\epsilon_L = \epsilon_L^{(v)} + \epsilon_L^{(c)} \quad \tilde{\epsilon}_L = -\hat{\alpha}'_{\varphi\varphi} \tag{2.8a}$$

$$\epsilon_L^{(v)} = 2\hat{\alpha}_{\varphi l}^{(3)} + 2 \frac{[V (\hat{\alpha}_{\varphi q}^{(3)})^\dagger]_{11}}{V_{ud}} + 4\hat{\alpha}_{\varphi l}^{(3)} \frac{[V (\hat{\alpha}_{\varphi q}^{(3)})^\dagger]_{11}}{V_{ud}} \tag{2.8b}$$

$$\epsilon_L^{(c)} = -2 \frac{[V \hat{\alpha}_{lq}^{(3)}]_{11}}{V_{ud}} \tag{2.8c}$$

$$\epsilon_R = -\frac{[\hat{\alpha}_{\varphi\varphi}]_{11}}{V_{ud}} \quad \tilde{\epsilon}_R = -\frac{[\hat{\alpha}_{e\nu ud}]_{11}}{V_{ud}} \tag{2.8d}$$

$$\epsilon_S - \epsilon_P = -2 \frac{[V \hat{\alpha}_{qde}^\dagger]_{11}}{V_{ud}} \quad \tilde{\epsilon}_S - \tilde{\epsilon}_P = 2 \frac{[V \hat{\alpha}'_{lq}]_{11}}{V_{ud}} \tag{2.8e}$$

$$\epsilon_S + \epsilon_P = -2 \frac{[\hat{\alpha}_{lq}^\dagger]_{11}}{V_{ud}} \quad \tilde{\epsilon}_S + \tilde{\epsilon}_P = -2 \frac{[\hat{\alpha}_{qu\nu}]_{11}}{V_{ud}} \tag{2.8f}$$

$$\epsilon_T = -\frac{[\hat{\alpha}_{lq}^{t\dagger}]_{11}}{V_{ud}} \quad \tilde{\epsilon}_T = \frac{[V \hat{\alpha}_{lq}^{t\dagger}]_{11}}{V_{ud}}. \tag{2.8g}$$

In the above matching conditions  $V$  denotes the CKM matrix, and the quark family indices “11” are explicitly displayed. The  $\alpha$  coefficients are defined in a flavor basis where both the down-quark and charged lepton Yukawa matrices are diagonal.

---

<sup>1</sup>We split the correction  $\epsilon_L$  to the SM operator into a vertex correction  $\epsilon_L^{(v)}$  and a contact correction  $\epsilon_L^{(c)}$  originating from a four-fermion weak scale operator. In the vertex correction  $\epsilon_L^{(v)}$  we include both linear and quadratic new physics effects.

We note here that while the physical amplitudes are renormalization scale and scheme independent, the individual effective couplings  $\epsilon_{S,P,T}$  ( $\tilde{\epsilon}_{S,P,T}$ ) and the corresponding hadronic matrix elements can display a strong scale dependence. Throughout the paper, we will quote estimates and bounds for the  $\epsilon_i$  ( $\tilde{\epsilon}_i$ ) at the renormalization scale  $\mu = 2$  GeV in the  $\overline{MS}$  scheme.

### 2.3 Nucleon-level effective couplings

The quark-level effective Lagrangian (2.7) can be matched onto a nucleon-level effective Lagrangian by computing the one-nucleon matrix elements of all quark bilinears. To leading order in momentum transfer one has  $\langle p | \bar{u} \Gamma d | n \rangle = g_\Gamma \bar{\psi}_p \Gamma \psi_n$  with  $\Gamma = 1, \gamma_5, \gamma_\mu, \gamma_\mu \gamma_5, \sigma_{\mu\nu}$ , and one then recovers the Lee-Yang [6] effective Lagrangian. The Lee-Yang [6] effective couplings  $C_i, C'_i$  ( $i \in \{V, A, S, T\}$ ) can be expressed in terms of our parameters as

$$C_i = \frac{G_F}{\sqrt{2}} V_{ud} \bar{C}_i \quad (2.9a)$$

$$\bar{C}_V = g_V (1 + \epsilon_L + \epsilon_R + \tilde{\epsilon}_L + \tilde{\epsilon}_R) \quad (2.9b)$$

$$\bar{C}'_V = g_V (1 + \epsilon_L + \epsilon_R - \tilde{\epsilon}_L - \tilde{\epsilon}_R) \quad (2.9c)$$

$$\bar{C}_A = -g_A (1 + \epsilon_L - \epsilon_R - \tilde{\epsilon}_L + \tilde{\epsilon}_R) \quad (2.9d)$$

$$\bar{C}'_A = -g_A (1 + \epsilon_L - \epsilon_R + \tilde{\epsilon}_L - \tilde{\epsilon}_R) \quad (2.9e)$$

$$\bar{C}_S = g_S (\epsilon_S + \tilde{\epsilon}_S) \quad (2.9f)$$

$$\bar{C}'_S = g_S (\epsilon_S - \tilde{\epsilon}_S) \quad (2.9g)$$

$$\bar{C}_P = g_P (\epsilon_P - \tilde{\epsilon}_P) \quad (2.9h)$$

$$\bar{C}'_P = g_P (\epsilon_P + \tilde{\epsilon}_P) \quad (2.9i)$$

$$\bar{C}_T = 4 g_T (\epsilon_T + \tilde{\epsilon}_T) \quad (2.9j)$$

$$\bar{C}'_T = 4 g_T (\epsilon_T - \tilde{\epsilon}_T) . \quad (2.9k)$$

Using these relations and the results of Ref. [7] one can work out the dependence of neutron and nuclear beta decay observables on the short-distance parameters  $\epsilon_i$  and  $\tilde{\epsilon}_i$ .

The vector charge  $g_V = 1$  up to tiny second-order isospin-breaking corrections. First principle calculations of  $g_{A,S,P,T}$  are nowadays possible with lattice QCD (LQCD). The status of LQCD calculations of these charges is critically reviewed in [8], where the first estimate of  $g_S$  from LQCD was provided. For the axial coupling  $g_A$ , the upshot is that different calculations give results in the range  $1.12 < g_A < 1.26$ , with errors much larger than the one achieved in the experimental determination [9]. New lattice analyses of the scalar and tensor charge have been recently performed. Ref. [8] reported  $g_S = 0.8 \pm 0.4$  and  $g_T = 1.05 \pm 0.35$  in the  $\overline{MS}$  scheme and at  $\mu = 2$  GeV, where the uncertainties include an estimate of all the systematic effects (volume, lattice spacing, and chiral extrapolations). More recently Ref. [10] provided improved results for the scalar and tensor charges,  $g_S = 1.08 \pm 0.28$  and  $g_T = 1.038 \pm 0.011$ , with uncertainty associated with statistics and chiral extrapolation. These results, however, do not include an estimate of the systematic

error associated with finite volume and finite lattice spacing extrapolations. Therefore, in what follows we will still use the results of Ref. [8] as baseline lattice results.

### 3 Low energy bounds

The couplings  $\epsilon_\alpha$  and  $\tilde{\epsilon}_\beta$  appearing in the Lagrangian (2.7) have been traditionally constrained through low-energy probes, such as decays of the pion, the neutron, and nuclei. Detailed analyses of these low-energy bounds can be found in Refs. [3, 2, 11, 8]. Here we present a brief survey of current and future constraints using the notation introduced in the previous section.

The ten non-standard couplings can be divided in two classes: the  $\epsilon_\alpha$  that involve L-handed neutrinos, and the  $\tilde{\epsilon}_\beta$  that involve R-handed neutrinos. The  $\tilde{\epsilon}_\beta$  appear in decay rates and distributions either quadratically or multiplied by the small factor  $m_\nu/E_\nu$  (through interference of the SM and BSM couplings). On the other hand, the  $\epsilon_\alpha$  couplings contribute to decay rates to linear order without any suppression. As a consequence, the low-energy bounds on the  $\epsilon$ 's will be stronger than the bounds on the  $\tilde{\epsilon}$ 's.

Experiments constrain the products of hadronic matrix elements and quark-level NP couplings  $\epsilon_i$  and  $\tilde{\epsilon}_i$ , or linear combinations of these products. The confidence intervals on the  $\epsilon_i$  and  $\tilde{\epsilon}_i$  are obtained using the so-called R-Fit method [12], which assumes that the matrix elements are bound to remain within allowed ranges determined by the analytical or numerical calculations.<sup>2</sup> We now discuss in turn the low-energy bounds on the  $\epsilon$ 's and  $\tilde{\epsilon}$ 's, and summarize the results in Tables 5 and 6.

**Vector and axial couplings:** The combinations  $(\epsilon_L \pm \epsilon_R)$  affect the overall normalization of the effective Fermi constant in processes mediated by the vector and axial-vector current, respectively. The hadronic matrix elements of the vector current are known very precisely through QCD flavor symmetry considerations (SU(2) and SU(3)), while the axial-vector matrix elements require non-perturbative calculations. Therefore, while the combination  $(\epsilon_L - \epsilon_R)$  remains relatively poorly unconstrained,  $(\epsilon_L + \epsilon_R)$  is strongly constrained by quark-lepton universality tests (or CKM unitarity tests) [11], that involve a precise determination of  $V_{ud}$  and  $V_{us}$  from processes mediated by the vector current (such as  $0^+ \rightarrow 0^+$  nuclear decays and  $K \rightarrow \pi \ell \nu$ ). Assuming that one operator at the time dominates, CKM unitarity constraints impose severe bounds on  $\epsilon_L^{(v)}$ ,  $\epsilon_L^{(c)}$ ,  $\epsilon_R$ . The bound on the vertex correction  $\epsilon_L^{(v)}$  is comparable to the one obtained by  $Z$ -pole observables [11], while the bounds on  $\epsilon_L^{(c)}$  and  $\epsilon_R$  are stronger than from any other source. Independent handles on  $\epsilon_R$  are not possible because neutron and nuclear correlation decay experiments are only sensitive to the combination  $(1 - 2\epsilon_R)g_A/g_V$ , so that disentangling  $\epsilon_R$  requires precision measurements of  $(1 - 2\epsilon_R)g_A/g_V$  and precision calculations of  $g_A/g_V$  in LQCD, which are not yet at the required sub-percent level.

---

<sup>2</sup>In the case at hand the relevant ranges are  $0.4 \leq g_S \leq 1.2$  and  $0.7 \leq g_T \leq 1.4$  for the nucleon matrix elements [8] and  $0.20 \leq f_T \leq 0.28$  for meson form factor appearing in the radiative pion decay [13].

**Pseudoscalar coupling:** The effective pseudoscalar coupling  $\epsilon_P$  contributes to leptonic decays of the pion  $\pi \rightarrow \ell \nu_\ell$ . Strong constraints are implied by the helicity-suppressed ratio  $R_\pi \equiv \Gamma(\pi \rightarrow e \nu[\gamma])/\Gamma(\pi \rightarrow \mu \nu[\gamma])$  [14, 15, 16], assuming that the coupling  $\epsilon_P$  is independent of the lepton masses (in particular that they do not satisfy  $\epsilon_P^{(e)}/m_e = \epsilon_P^{(\mu)}/m_\mu$ ). Even after taking into account possible cancellations between flavor diagonal and non-diagonal contributions one obtains the strong bound reported in Table 5 (for details see [8]).

**Scalar and tensor couplings:** The scalar and tensor couplings  $\epsilon_S$  and  $\epsilon_T$  contribute to linear order to the Fierz interference terms in beta decays of neutrons and nuclei, and to the neutrino-asymmetry correlation coefficient  $B$  in polarized neutron and nuclear decays. Because of the peculiar way in which the Fierz interference term appears in many asymmetry measurements, bounds on  $\epsilon_S$  and  $\epsilon_T$  can also be obtained by observation of the beta-asymmetry correlation coefficient  $A$ , electron-neutrino correlation  $a$ , and positron polarization measurements in various nuclear beta decays. Currently, the most stringent constraint on  $\epsilon_S$  arises from the Fierz interference term in  $0^+ \rightarrow 0^+$  nuclear beta decays ( $-0.001 < g_S \epsilon_S < 0.0032$  at 90% CL) [17], while the strongest constraint on  $\epsilon_T$  arises from a Dalitz-plot analysis of the radiative pion decay  $\pi \rightarrow e \nu \gamma$  [18, 13] ( $-2.0 \times 10^{-4} < \epsilon_T f_T < 2.6 \times 10^{-4}$  at 90% CL).

Moreover, as discussed in Refs. [19, 20, 21] and summarized in [8], there are also potentially very strong constraints on  $\epsilon_{S,T}$  from  $R_\pi \equiv \Gamma(\pi \rightarrow e \nu[\gamma])/\Gamma(\pi \rightarrow \mu \nu[\gamma])$ , due to operator mixing: once a scalar or tensor interaction is generated by new physics, SM radiative corrections will generate an effective pseudoscalar operator that mediates the helicity-suppressed modes. Numerically, the bounds are at the level of  $|\epsilon_S| \lesssim 8 \times 10^{-2}$  and  $|\epsilon_T| \lesssim 10^{-3}$ , almost as strong as the “direct” bounds discussed above. It is important to keep in mind, however, that if the flavor structure of the SM extension is known, this constraint could be the strongest.

In the future,  $10^{-3}$ -level measurements of the antineutrino asymmetry in neutron decay [22, 23], and the Fierz interference term in neutron decay [24, 25] and in the pure Gamow-Teller decay of  ${}^6\text{He}$  [26] will probe  $\epsilon_T$  in the  $5 \times 10^{-4}$  range.

**Couplings involving R-handed neutrinos ( $\tilde{\epsilon}_\alpha$ ):** Neglecting neutrino masses, all the  $\tilde{\epsilon}_\beta$  couplings contribute to decay rates incoherently with the SM, i.e.  $\propto |\tilde{\epsilon}_\beta|^2$ . Detailed expressions of the contributions to neutron and nuclear beta decay correlation coefficients can be found in [27] (one needs to re-express the Lee-Yang couplings in terms of the  $\epsilon_\alpha$  and  $\tilde{\epsilon}_\beta$  using Eqs 2.9 above). The corresponding bounds can be obtained from the analysis of Ref. [2], in particular from the fits to beta decay data allowing for non-zero  $\tilde{\epsilon}_L, \tilde{\epsilon}_R$  only, implying  $|\tilde{\epsilon}_L \pm \tilde{\epsilon}_R| < 0.06$ , and  $\tilde{\epsilon}_S, \tilde{\epsilon}_T$  only, implying  $|g_S \tilde{\epsilon}_S| < 0.06$ ,  $|g_T \tilde{\epsilon}_T| < 0.02$  at 90% CL.

The ratio of leptonic pion decay rates  $R_\pi \equiv \Gamma(\pi \rightarrow e \nu[\gamma])/\Gamma(\pi \rightarrow \mu \nu[\gamma])$  is a very sensitive probe of the pseudoscalar coupling  $\tilde{\epsilon}_P$  and through operator mixing can also constrain  $\tilde{\epsilon}_S, \tilde{\epsilon}_T$ . Assuming possible cancellations between  $\epsilon_P$  and  $\tilde{\epsilon}_P$  (see discussion in Ref. [8] with the replacement  $\epsilon_P^{ex} \rightarrow \tilde{\epsilon}_P^{ee}$ ), one obtains  $|\tilde{\epsilon}_P| < 2.8 \times 10^{-4}$ . The mixing

constraint can be worked out by using the three-operator mixing results from Ref. [21], namely:<sup>3</sup>

$$\tilde{\epsilon}_P(\mu) = \tilde{\epsilon}_P(\Lambda) \left( 1 + \gamma_{PP} \log \frac{\Lambda}{\mu} \right) + \tilde{\epsilon}_S(\Lambda) \gamma_{SP} \log \frac{\Lambda}{\mu} + \tilde{\epsilon}_T(\Lambda) \gamma_{TP} \log \frac{\Lambda}{\mu} \quad (3.1a)$$

$$\gamma_{PP} = \frac{3}{4} \frac{\alpha_2}{\pi} + \frac{49}{144} \frac{\alpha_1}{\pi} \approx 8.6 \times 10^{-3} \quad (3.1b)$$

$$\gamma_{SP} = \frac{3}{16} \frac{\alpha_1}{\pi} \approx 0.6 \times 10^{-3} \quad (3.1c)$$

$$\gamma_{TP} = \frac{9}{2} \frac{\alpha_2}{\pi} - \frac{1}{3} \frac{\alpha_1}{\pi} \approx +4.4 \times 10^{-2}, \quad (3.1d)$$

where  $\alpha_1 = \alpha/\cos^2 \theta_W$  and  $\alpha_2 = \alpha/\sin^2 \theta_W$  are the  $U(1)$  and  $SU(2)$  weak couplings, expressed in terms of the fine-structure constant and the weak mixing angle. Setting  $\tilde{\epsilon}_P(\Lambda) = 0$  and neglecting the small  $O(\alpha/\pi)$  fractional difference between  $\tilde{\epsilon}_{S,T}(\Lambda)$  and the observable  $\tilde{\epsilon}_{S,T}(\mu)$  at the low scale, the 90% C.L. constraint on the  $\tilde{\epsilon}_S$ - $\tilde{\epsilon}_T$  plane reads

$$|0.6 \tilde{\epsilon}_S + 44.2 \tilde{\epsilon}_T| \leq \frac{0.28}{\log(\Lambda/\mu)}. \quad (3.2)$$

Assuming  $\log(\Lambda/\mu) \sim 10$  (e.g.  $\Lambda \sim 10$  TeV and  $\mu \sim 1$  GeV), we get  $|\tilde{\epsilon}_S| \lesssim 5 \times 10^{-2}$  and  $|\tilde{\epsilon}_T| \lesssim 0.6 \times 10^{-3}$ , which are the strongest low-energy bounds on the  $\tilde{\epsilon}$ 's couplings. However, given the dependence of these results on assumptions about the flavor structure of the couplings, we do not report these bounds in Table 6. It is worth pointing out that the LHC bound on  $\tilde{\epsilon}_S$  derived in the next section and shown in Table 6 is a factor four stronger than this bound from  $R_\pi$ .

## 4 Collider bounds

Collider searches can also probe the various non-standard couplings  $\epsilon_\alpha$  and  $\tilde{\epsilon}_\beta$  defined above. In Ref. [8] bounds were derived on  $\epsilon_{S,T}$  by analyzing LHC data in the  $pp \rightarrow e + MET + X$  channel at  $\sqrt{s} = 7$  TeV and  $1 \text{ fb}^{-1}$  integrated luminosity. Here we extend the analysis to all non-standard charged-current couplings and we consider bounds from both  $pp \rightarrow e + MET + X$  and  $pp \rightarrow e^+e^- + X$  channels (using  $SU(2)$  gauge invariance).

As in Ref. [8], here our analysis is to lowest order (LO) in the QCD interactions. While QCD effects have a small impact on the transverse mass distribution [28], their impact on the overall normalization ( $K$ -factor) and dilepton invariant mass distributions of the NP interactions are not known and affects our analysis at the order  $\alpha_s/\pi$ . To maintain an analysis consistent to the same order in the QCD interactions, we therefore do not include a  $K$ -factor in our projections of the background. For our analyses of existing data we use background estimates provided by the experimental collaborations.

---

<sup>3</sup>There is a typo in Eqs. (25-26) of Ref. [21], where the definitions of the operators  $O_1$  and  $O_2$  should be interchanged.



## 4.1 The $pp \rightarrow e + MET + X$ channel

This channel is directly related to beta decays, since the parton-level process is  $\bar{u}d \rightarrow e\bar{\nu}$ . We will use the (cumulative) transverse mass distribution to put bounds on the non-standard interactions. Including the  $W$ -exchange Standard Model contribution, to leading order (LO) in QCD the  $pp \rightarrow e\nu + X$  cross-section for lepton transverse mass  $m_T \equiv \sqrt{2E_T^e E_T^\nu (1 - \cos \Delta\phi_{e\nu})}$  greater than a threshold  $\bar{m}_T$  takes the following form<sup>4</sup>:

$$\begin{aligned} \sigma(m_T > \bar{m}_T) &= \sigma_W \left[ (1 + \epsilon_L^{(v)})^2 + |\tilde{\epsilon}_L|^2 + |\epsilon_R|^2 \right] - 2\sigma_{WL} \epsilon_L^{(c)} \left( 1 + \epsilon_L^{(v)} \right) \\ &+ \sigma_R \left[ |\tilde{\epsilon}_R|^2 + |\epsilon_L^{(c)}|^2 \right] + \sigma_S \left[ |\epsilon_S|^2 + |\tilde{\epsilon}_S|^2 + |\epsilon_P|^2 + |\tilde{\epsilon}_P|^2 \right] \\ &+ \sigma_T \left[ |\epsilon_T|^2 + |\tilde{\epsilon}_T|^2 \right], \end{aligned} \quad (4.1)$$

where, defining  $\bar{\tau} = \bar{m}_T^2/s$ , the individual contributions  $\sigma_i$  ( $i \in \{W, WL, R, S, T\}$ ) read

$$\sigma_i = \frac{|V_{ud}|^2}{192\pi} \frac{s}{v^4} \int_{\bar{\tau}}^1 d\tau L(\tau) \sqrt{\tau(\tau - \bar{\tau})} g_i(\tau) \quad (4.2a)$$

$$g_W(\tau) = \frac{8}{3} \frac{M_W^4}{s^2} \frac{1 - \frac{\bar{\tau}}{4\tau}}{\left(\tau - \frac{M_W^2}{s}\right)^2 + \frac{\Gamma_W^2}{s} \frac{M_W^2}{s}} \quad (4.2b)$$

$$g_{WL}(\tau) = g_W(\tau) \frac{s}{M_W^2} \left( \tau - \frac{M_W^2}{s} \right) \quad (4.2c)$$

$$g_R(\tau) = \frac{8}{3} \left( 1 - \frac{\bar{\tau}}{4\tau} \right) \quad (4.2d)$$

$$g_S(\tau) = 1 \quad (4.2e)$$

$$g_T(\tau) = \frac{32}{3} \left( 1 - \frac{\bar{\tau}}{\tau} \right) \quad (4.2f)$$

$$L(\tau) = \int_{\frac{1}{2} \ln \tau}^{-\frac{1}{2} \ln \tau} dy_P \left[ f_{\bar{u}}(\sqrt{\tau} e^{y_P}) f_d(\sqrt{\tau} e^{-y_P}) + (\bar{u}, d) \rightarrow (u, \bar{d}) \right]. \quad (4.2g)$$

The various contributions to  $\sigma(m_T > \bar{m}_T)$  are plotted in Fig. 1 using the CTEQ6 set of parton distribution functions (PDF) in the  $\overline{MS}$  scheme, referred to as CTEQ6M, evaluated at  $Q^2 = 1 \text{ TeV}^2$  [29]. In the Figure we see a clear hierarchy that determines the sensitivity to the different kind of new interactions: the NP couplings that appear multiplying  $\sigma_W$  in Eq. (4.1) will be essentially unconstrained by this analysis, since they do not have any enhancement with respect to the SM background, whereas for the rest of

---

<sup>4</sup>The interference of (pseudo)scalar and tensor interactions vanishes after integration over the final leptons rapidities if the integration region is symmetric (under the exchange of both rapidities), as it happens in the absence of any cut. However experimental cuts break this symmetry (see later in this section) generating a residual contribution from these interference terms. We find the relative contribution to be numerically small.

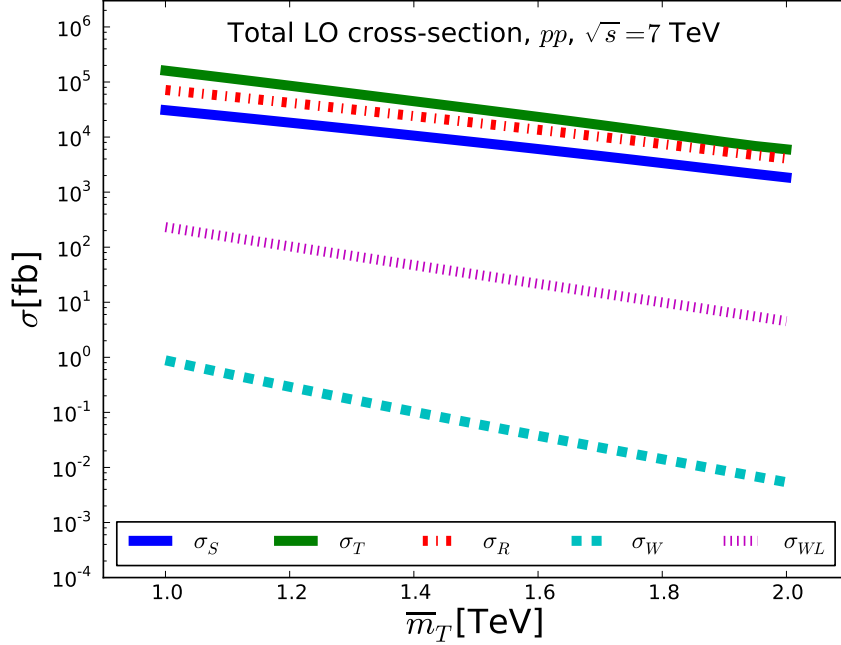


Figure 1: Cross-sections introduced in Eq. (4.1) as a function of the cut on the transverse mass  $\bar{m}_T$ , for  $\sqrt{s} = 7$  TeV. We see that in the entire plot range we have the hierarchy  $\sigma_T > \sigma_R > \sigma_S \gg \sigma_{WL} \gg \sigma_W$ .

the NP couplings we obtain strong bounds. One important feature emerging from Fig. 1 is that the SM term  $\sigma_W$  goes to zero faster than the rest of terms, thus implying that larger values of the transverse mass cut  $\bar{m}_T$  increase the signal/background ratio.

Writing  $\sigma(m_T > \bar{m}_T) = \sigma_W + \sigma_{NP}(\epsilon_\alpha)$ , and using the current CMS and ATLAS results on  $pp \rightarrow e\nu + X$ , one can put bounds on the couplings  $\epsilon_\alpha$ . For a given number of expected background events  $n_b$  and actually observed events  $n$ , the 90% C.L. upper bound on the number of NP signal events  $n_s^{up}$  can be calculated using [9]

$$0.10 = e^{-n_s^{up}} \cdot \frac{\sum_{m=0}^n \frac{1}{m!} (n_s^{up} + n_b)^m}{\sum_{m=0}^n \frac{1}{m!} n_b^m}, \quad (4.3)$$

which implies  $\sigma_{NP} < n_s^{up}/(\epsilon_{eff} L)$ , where  $\epsilon_{eff}$  represents the acceptance ( $\epsilon_A$ )<sup>5</sup> times the lepton detection efficiency factor ( $\epsilon_{det}$ ), and  $L$  is the integrated luminosity.

We use for our study the most recent analysis of this channel published by the CMS Collaboration [30], with  $5 \text{ fb}^{-1}$  at  $\sqrt{s} = 7$  TeV. The observed and expected number of events above the chosen cut on the transverse mass, and the associated upper bound on NP signal events  $n_s^{up}$ , are given in Table 1. Also shown are analogous numbers based on  $20 \text{ fb}^{-1}$  of integrated luminosity at  $\sqrt{s} = 8$  TeV. To make this projection we assume no events are detected. This is a reasonable assumption, since from a LO computation of  $pp \rightarrow W^* \rightarrow e\nu$  we expect  $\sim 0.3$  background events for  $\bar{m}_T = 2$  TeV.

<sup>5</sup> For the processes that we are studying, CMS performs the following cuts on the rapidities  $y, y'$  of the charged leptons: (i)  $|y, y'| < 2.5$ ; (ii)  $|y, y'| \notin (1.442, 1.560)$  (the transition region between barrel and endcaps); and for the dilepton search, in addition (iii) CMS rejects events in which both leptons are in the endcap regions.

|       | Reference  | $\sqrt{s}$ (TeV) | $\mathcal{L}$ (fb $^{-1}$ ) | $\overline{m}_T$ (TeV) | $n$ | $n_b$         | $n_s^{up}$ |
|-------|------------|------------------|-----------------------------|------------------------|-----|---------------|------------|
| LHC-7 | CMS [30]   | 7                | 5.0                         | 1.2                    | 3   | $2.8 \pm 1.0$ | 4.5        |
| LHC-8 | Projection | 8                | 20                          | 2.0                    | 0   | $< 1$         | 2.3        |

Table 1: Experimental data (real or expected) and cuts over the transverse mass used in our analysis of  $pp \rightarrow e + MET + X$ .  $n$  ( $n_b$ ) is the number of observed (background) events, and  $n_s^{up}$  is the 90% CL upper limit on the number of signal events. For the projection no events are assumed to be observed.

The acceptance  $\epsilon_A$  of the signal is set by the rapidity coverage of the detector and the kinematic cuts applied at the analysis-level. While the CMS analysis does have such additional cuts, to LO in the QCD interactions these have 100% acceptance on the signal, such that the acceptance is almost entirely given by the geometric acceptance  $\epsilon_{geom}$  of the lepton. We find a very high geometric acceptance, in the range 97-100% (the lowest value being associated with the tensor-induced cross-section  $\sigma_T$ ). The variance between interactions is at most a couple of percent, and the dependence on  $\overline{m}_T$  or  $\sqrt{s}$  is mild. The reason for these features is simply because for such high values of  $\overline{m}_T$  the lepton is almost always central.

Next, we infer from [30] a lepton detection efficiency of  $\sim 90\%$ . Taken together, for our analysis we therefore use  $\epsilon_{eff} \approx 0.87$ . It is worth noting that varying  $\epsilon_{eff}$  through the range of 0.7 – 1.0, the NP bounds presented below are modified by only O(20%), which is at the same level as the PDF and NLO QCD uncertainties.

|       | $ \epsilon_{S,P} ,  \tilde{\epsilon}_{S,P} $ | $ \epsilon_T ,  \tilde{\epsilon}_T $ | $ \tilde{\epsilon}_R $ | $\epsilon_L^{(c)}$            |
|-------|----------------------------------------------|--------------------------------------|------------------------|-------------------------------|
| LHC-7 | $1.3 \times 10^{-2}$                         | $2.9 \times 10^{-3}$                 | $4.9 \times 10^{-3}$   | $(-3.1, +8.0) \times 10^{-3}$ |
| LHC-8 | $0.9 \times 10^{-2}$                         | $2.2 \times 10^{-3}$                 | $3.4 \times 10^{-3}$   | $(-2.5, +4.6) \times 10^{-3}$ |

Table 2: LHC bounds (first row) and projected bounds (second row) at 90% C.L., on  $\epsilon_i$  and  $\tilde{\epsilon}_i$  ( $i = S, P, T, R$ ) at the renormalization scale  $\mu = 2$  GeV in the  $\overline{\text{MS}}$  scheme using the information given in Table 1.

Putting the above results together, the bounds on the different NP coefficients are given in Table 2. These results are obtained using the CTEQ6M parton distribution functions [29] at  $Q^2 = 1$  TeV $^2$ . To estimate the uncertainty in these bounds arising from the parton distribution functions, we also used the MSTW2008 PDF sets [31] and obtained bounds that differ by O(10%) from those presented in the Table 2. We also find comparable bounds from the the ATLAS 4.7 fb $^{-1}$   $e + MET + X$  analysis at  $\sqrt{s} = 7$  TeV [32], as well as from the CMS 3.7 fb $^{-1}$  analysis at  $\sqrt{s} = 8$  TeV [33].

Note that since collider searches set limits on the effective couplings  $\epsilon_i$  and  $\tilde{\epsilon}_i$  at the high renormalization scale  $\mu = 1$  TeV, a direct comparison with the low-energy constraints requires an appropriate rescaling down to the hadronic scale. Using the one-loop anomalous dimensions for the different quark bilinears (see [34] and references therein), the one-loop beta function for the strong coupling constant, and including the appropriate heavy quark thresholds, we find in the  $\overline{\text{MS}}$  scheme  $\epsilon_{S,P}(1 \text{ TeV})/\epsilon_{S,P}(2 \text{ GeV}) = 0.56$

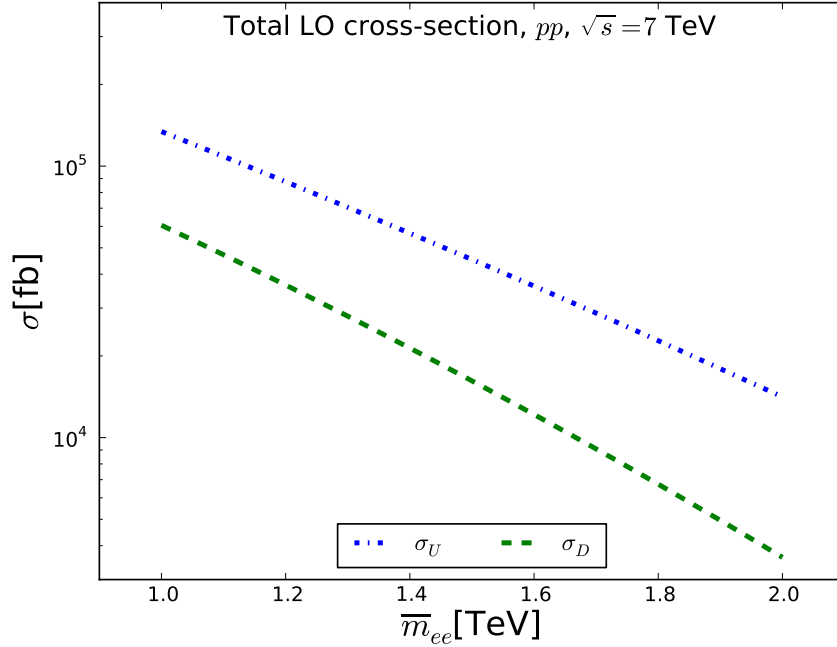


Figure 2: Cross-sections  $\sigma_{u,d}$  defined in Eq. (4.6) versus the cut  $\overline{m}_{ee}$  over the dilepton invariant mass.

and  $\epsilon_T(1 \text{ TeV})/\epsilon_T(2 \text{ GeV}) = 1.21$ , whereas  $\epsilon_{L,R}$  are the same at both scales since the associated bilinears have zero anomalous dimension<sup>6</sup>. These factors have already been taken into account in the results shown in Table 2.

These bounds have been obtained assuming contributions from one operator at a time and one might wonder about possible cancellations when several NP terms are present. For that matter, first of all one should notice that all the contributions to  $\sigma_{NP}$  are positive-definite, except for those generated by  $\epsilon_L^{(v,c)}$ , where a negative contribution due to destructive interference with the SM amplitude (or among the NP terms) is possible. However, the constraints on these NP terms from LEP and CKM-unitarity tests are very strong:  $|\epsilon_L^{(v,c)}| < 5 \cdot 10^{-4}$  at 90% C.L. [11], and this leaves room only for a very small negative contribution in  $\sigma_{NP}$ , that would weaken our bounds on the other NP couplings at most by a few percent.

## 4.2 The $pp \rightarrow e^+e^- + X$ channel

$SU(2)$  gauge invariance implies that some of the 4-fermi operators (2.4) and vertex correction operators (2.5) mediate the transitions  $q\bar{q} \rightarrow e^+e^-$  and/or  $q\bar{q} \rightarrow \nu\bar{\nu}$  ( $q = u, d$ ). At the LHC the first transition contributes to the Drell-Yan process  $pp \rightarrow e\bar{e} + X$ , while the second one contributes to a mono-jet signal arising from the parton-level process  $q\bar{q} \rightarrow \nu\bar{\nu} + g$ . Because this parton-level process involves one additional perturbative vertex, we expect weaker bounds from the mono-jets searches, and focus therefore on the Drell-Yan process  $pp \rightarrow e\bar{e} + X$ .

<sup>6</sup>The  $\tilde{\epsilon}_i$  couplings run under QCD in the same way as the  $\epsilon_i$ .

In what follows we additionally focus on those operators that involve a chirality-flip. Then the relevant interaction Lagrangian is given by

$$\mathcal{L}_{\text{NC}} = \frac{\delta_{P-S}}{v^2} \bar{e}_R e_L \bar{d}_L d_R + \frac{\delta_{P+S}}{v^2} \bar{e}_R e_L \bar{u}_R u_L + \frac{\delta_T}{v^2} \bar{e}_R \sigma_{\mu\nu} e_L \bar{u}_R \sigma^{\mu\nu} u_L + \text{h.c.} , \quad (4.4)$$

where  $\delta_{P-S} = [\hat{\alpha}_{qde}^\dagger]_{11}$ ,  $\delta_{P+S} = -[\hat{\alpha}_{ql}^\dagger V^\dagger]_{11}$ ,  $\delta_T = -[\hat{\alpha}_{ql}^{t\dagger} V^\dagger]_{11}$ . These effective couplings  $\delta_{S\pm P, T}$  differ from the couplings  $\epsilon_{S\pm P, T}$  that contribute to beta decays at low energy and  $pp \rightarrow e\nu + X$  at the LHC.

However a simple relation arises in the generic case in which (i) all  $\hat{\alpha}_{ij}$  are of the same order; (ii) the off-diagonal entries  $\hat{\alpha}_{i\neq j}$  are suppressed compared to the diagonal entries:

$$\delta_{P-S} = \frac{\epsilon_P - \epsilon_S}{2} \quad \delta_{P+S} = \frac{\epsilon_P + \epsilon_S}{2} |V_{ud}|^2 \quad \delta_T = \epsilon_T |V_{ud}|^2 . \quad (4.5)$$

Under these weak assumptions on the flavor structure of the new-physics couplings, we now use the Drell-Yan process to obtain bounds on  $\epsilon_S \pm \epsilon_P$  and  $\epsilon_T$ .

To leading order in strong interactions, the NP contribution to the cross-section for  $pp \rightarrow e^+e^- + X$  with di-lepton invariant mass  $m_{ee} > \bar{m}_{ee}$  reads

$$\sigma_{NP}(m_{ee} > \bar{m}_{ee}) = \sigma_u \left[ |\delta_{P+S}|^2 + \frac{16}{3} |\delta_T|^2 \right] + \sigma_d |\delta_{P-S}|^2 , \quad (4.6a)$$

$$\sigma_{u,d} = \frac{1}{48\pi} \frac{s}{v^4} \int_{\bar{\tau}}^1 d\tau \tau \tilde{L}_{u,d}(\tau) , \quad (4.6b)$$

$$\tilde{L}_q(\tau) = \int_{\frac{1}{2} \ln \tau}^{-\frac{1}{2} \ln \tau} dy_P f_q(\sqrt{\tau} e^{y_P}) f_{\bar{q}}(\sqrt{\tau} e^{-y_P}) , \quad (4.6c)$$

where  $\bar{\tau} = \bar{m}_{ee}^2/s$ . The  $\sigma_{u,d}(\bar{m}_{ee})$  functions are shown in Fig. 2, using the CTEQ6M PDF set.

Exactly in the same way as it was done for the  $pp \rightarrow e\nu$  channel in the previous section, we obtain bounds on the NP couplings  $\delta_\alpha$  by requiring the number of NP signal events  $n_s$  to be smaller than the 90% C.L. upper bound  $n_s^{up}$ , i.e.  $\sigma_{NP} < n_s^{up}/(\epsilon_{eff} L)$ . In order to do that, we use results from the analysis of 5 fb<sup>-1</sup> of dilepton data at  $\sqrt{s} = 7$  TeV given by the CMS Collaboration [35]. The relevant data and details of their analysis are given in Table 3.

|       | Reference      | $\sqrt{s}$ | $\mathcal{L}$        | $m_{ee}$ | $n$ | $n_b$ | $n_s^{up}$ |
|-------|----------------|------------|----------------------|----------|-----|-------|------------|
| LHC-7 | CMS Coll. [35] | 7 TeV      | 5.0 fb <sup>-1</sup> | 1.35 TeV | 0   | -     | 2.3        |
| LHC-8 | Projection     | 8 TeV      | 20 fb <sup>-1</sup>  | 2.0 TeV  | 0   | < 1   | 2.3        |

Table 3: Experimental data (real or expected) and cuts over the dilepton invariant mass used in our analyses of the  $pp \rightarrow e^+e^- + X$  channel.  $n$  ( $n_b$ ) is the number of observed (background) events, and  $n_s^{up}$  is the 90% CL upper limit on the number of signal events.

Compared to the  $e + MET + X$  signature, here in the dilepton channel the geometric acceptances are lower, due to the reduced acceptance of the additional lepton compared

to the MET. For the scalar and pseduoscalar interactions we find at  $\sqrt{s} = 7$  TeV the geometric acceptance has a mild variation from  $\sim 87\% - 90\%$  as the cut on  $m_{ee}$  varies from 1 TeV to 1.6 TeV. The geometric acceptance of the tensor interaction is lower, and is almost constant at  $\sim 75\%$  across the same mass range. We find that the efficiencies are essentially unchanged in moving from  $\sqrt{s} = 7$  TeV to 8 TeV. Taking into account the dilepton detection efficiency of  $\approx 85\%$  [35], we find  $\epsilon_{eff} = 0.75$  for the  $\delta_{S\pm P}$  interactions, and  $\epsilon_{eff} = 0.65$  for the tensor interaction (see Table 4).

Using Eq. (4.5), we translate the bounds on  $\delta_{S,P,T}$  into bounds on  $\epsilon_{S,P,T}$ , assuming only one of these  $\epsilon$ 's is non-zero at a given time. These results are shown in Table 4. Also shown are estimates of future bounds that could be obtained with  $20 \text{ fb}^{-1}$  data at  $\sqrt{s} = 8$  TeV. To obtain these results we used Pythia 8.1 [36, 37] to generate background  $pp \rightarrow \gamma^*, Z^* \rightarrow ee + X$  events. Applying the rapidity selection cuts, a dilepton detection efficiency of 85%, and  $m_{ee} > 2.0$  TeV, we find  $\sim 0.2$  background events expected with  $20 \text{ fb}^{-1}$  of integrated luminosity. To obtain the projection for future bounds we therefore assumed that after all cuts no events will be detected.

The limits we obtain from current dilepton data are stronger than those from the  $pp \rightarrow e + MET$  data.

|       | $\epsilon_{det}$ | $\epsilon_{geom}(\delta_{S\pm P})$ | $\epsilon_{geom}(\delta_T)$ | $ \epsilon_{S,P} $   | $ \epsilon_T $       |
|-------|------------------|------------------------------------|-----------------------------|----------------------|----------------------|
| LHC-7 | $\sim 0.85$      | 0.90                               | 0.75                        | $1.0 \times 10^{-2}$ | $1.3 \times 10^{-3}$ |
| LHC-8 | 0.85 (assumed)   | 0.90                               | 0.75                        | $0.7 \times 10^{-2}$ | $0.9 \times 10^{-3}$ |

Table 4: LHC bounds (first row) and projected bounds (second row) at 90% C.L. for the new physics couplings  $\epsilon_{S,T,P}$  at the renormalization scale  $\mu = 2$  GeV in the  $\overline{\text{MS}}$  scheme, obtained from the  $pp \rightarrow e^+e^- + X$  channel, along with the detection efficiency and geometric acceptance.

### 4.3 Discussion of LHC bounds

We can summarize the results of this section as follows:

(i) We have updated the bounds on  $\epsilon_{S,T}$  obtained from the  $pp \rightarrow e + MET + X$  channel using  $5 \text{ fb}^{-1}$  of data (see Table 2), improving by  $\sim 25\%$  the bounds obtained with  $1 \text{ fb}^{-1}$  in Ref. [8].

(ii) We have extended this analysis to extract bounds on the other eight effective couplings  $\epsilon_i$  and  $\tilde{\epsilon}_i$  that describe non-standard CC weak interactions. We show that for  $\epsilon_{P,S,T}$ ,  $\tilde{\epsilon}_{P,S,T,R}$  and  $\epsilon_L^{(c)}$  the current bounds from an analysis of the  $pp \rightarrow e + MET + X$  channel at the LHC are at the 0.1%-1% level (see Table 2), whereas this search is essentially insensitive to the rest of couplings:  $\epsilon_R$ ,  $\epsilon_L^{(v)}$  and  $\tilde{\epsilon}_L$ .

(iii) We have studied the impact of  $pp \rightarrow e^+e^- + X$  in constraining the couplings  $\epsilon_{S,P,T}$ . This analysis relies on the use of  $SU(2)$  gauge invariance and very weak assumptions about the flavor structure of the theory. The resulting bounds on  $\epsilon_{S,P,T}$  are stronger than those obtained in the  $pp \rightarrow e + MET + X$  channel by a factor 1.3 and 2.3 for  $\epsilon_{S,P}$  and  $\epsilon_T$  respectively (compare Tables 2 and 4).

## 5 Conclusions

In this work we have analyzed all the phenomenological handles on the effective couplings  $\epsilon_i$  and  $\tilde{\epsilon}_i$  characterizing non-standard CC interactions. We have reviewed the limits on  $\epsilon_i$  and  $\tilde{\epsilon}_i$  from low energy experiments (nuclear and neutron  $\beta$  decays, CKM unitarity tests, pion decays, ...), and we have computed the bounds on the same couplings arising from LHC searches. This direct comparison relies on the assumption that the new physics mediating these new interactions arises at very high scale  $\Lambda > \text{few TeV}$ . Comparison of the best bounds available for each interaction from low- and high-energy experiments are shown in Tables 5 and 6, for the non-standard couplings involving left-handed and right-handed neutrinos, respectively. The main points can be summarized as follows:

- For the pseudo-scalar couplings  $\epsilon_P$  and  $\tilde{\epsilon}_P$  the low-energy constraints from pion decay are at the  $10^{-4}$  level, very hard to reach at the LHC in the near future. The same applies to the vector interactions  $\epsilon_L^{(c)}$ ,  $\epsilon_L^{(v)}$  and  $\epsilon_R$ , for which the 90% C.L. bound from CKM-unitarity (and LEP physics) is  $5 \times 10^{-4}$ ;
- For scalar and tensor interactions with left-handed neutrinos  $\epsilon_S$  and  $\epsilon_T$ , the low-energy experiments have been traditionally stronger, but the current LHC bounds have caught up and both probes are at the  $10^{-2}$  and  $10^{-3}$  level for  $\epsilon_S$  and  $\epsilon_T$  respectively. In the next few years we expect improvements in the bounds from both the LHC and low-energy, through neutron [22, 23, 24, 25] and  ${}^6\text{He}$  decay [26] measurements at the 0.1% level. These considerations imply that low-energy searches with  $10^{-4}$  sensitivity would have unmatched constraining potential, even in the LHC era.
- For scalar and tensor interactions with right-handed neutrinos  $\tilde{\epsilon}_S$  and  $\tilde{\epsilon}_T$ , the LHC bounds are also at the  $10^{-2}$  and  $10^{-3}$  level respectively, significantly better than current and future low-energy limits (to match the LHC bound one needs measurements of the electron-neutrino correlation “ $a$ ” in Gamow Teller transitions at the level of  $\delta a_{GT}/a_{GT} \sim 0.01\%$ )<sup>7</sup>. And the same conclusion applies to  $\tilde{\epsilon}_R$ , for which the LHC bound is  $5 \times 10^{-3}$  and no significant limit is available from low-energy probes;
- The remaining coefficient  $\tilde{\epsilon}_L$  cannot be probed at such a strong level by any of the mentioned experiments.

In conclusion, we have shown that by combining low-energy and LHC searches, a more complete and accurate picture of non-standard CC interactions emerges. As we discussed earlier, such a direct comparison is only possible if the new physics originates in the multi-TeV scale. The next natural question is: how robust are the above conclusions when the mediators of the new interactions are not heavy enough to be integrated out at LHC

---

<sup>7</sup>Within a given NP model the ratio  $\Gamma(\pi \rightarrow e\nu)/\Gamma(\pi \rightarrow \mu\nu)$  is likely to produce the strongest bound not only on  $\epsilon_P$  and  $\tilde{\epsilon}_P$ , but also on  $\epsilon_{S,T}$  and  $\tilde{\epsilon}_{S,T}$ , through their loop-induced contribution. However, as explained in Section 3 and Ref. [8], there is a loophole to this argument, because cancelations between different contributions can occur. For this reason in a general model-independent analysis the LHC provides the strongest constraint on  $\tilde{\epsilon}_{S,T}$ .

|                  | $ \epsilon_L^{(v)} $ | $\epsilon_L^{(c)}$ | $ \epsilon_R $ | $ \epsilon_P $ | $ \epsilon_S $ | $ \epsilon_T $ |
|------------------|----------------------|--------------------|----------------|----------------|----------------|----------------|
| Low energy       | 0.05                 | 0.05               | 0.05           | 0.06           | 0.8            | 0.1            |
| LHC ( $e\nu$ )   | -                    | (-0.3,+0.8)        | -              | 1.3            | 1.3            | 0.3            |
| LHC ( $e^+e^-$ ) | -                    | -                  | -              | 1.0            | 1.0            | 0.1            |

Table 5: Summary of 90% CL bounds (in units of  $10^{-2}$ ) on the non-standard couplings  $\epsilon_\alpha$  obtained from low-energy and LHC searches. In order to deduce the low-energy bound on the scalar coupling we used  $g_S = 0.8(4)$  [8]. Using  $g_S = 1.08(28)$  [10] would lead to the stronger bound  $|\epsilon_S| < 0.4 \times 10^{-2}$ .

|                | $ \tilde{\epsilon}_L $ | $ \tilde{\epsilon}_R $ | $ \tilde{\epsilon}_P $ | $ \tilde{\epsilon}_S $ | $ \tilde{\epsilon}_T $ |
|----------------|------------------------|------------------------|------------------------|------------------------|------------------------|
| Low energy     | 6                      | 6                      | 0.03                   | 14                     | 3.0                    |
| LHC ( $e\nu$ ) | -                      | 0.5                    | 1.3                    | 1.3                    | 0.3                    |

Table 6: Summary of 90% CL bounds (in units of  $10^{-2}$ ) on the non-standard couplings  $\tilde{\epsilon}_\alpha$  obtained from low-energy and LHC searches. In order to deduce the low-energy bounds on the scalar coupling we used  $g_S = 0.8(4)$  and  $g_T = 1.05(35)$  [8]. Using  $g_S = 1.08(28)$  [10] would lead to the stronger bound  $|\tilde{\epsilon}_S| < 6.9 \times 10^{-2}$ .

energies? In this case the EFT treatment of LHC data breaks down and the discussion becomes necessarily model-dependent. We leave investigations of explicit classes of models for future work.

## Acknowledgements

We thank Tanmoy Bhattacharya and Rajan Gupta for discussions, and Bruce Campbell for correspondence concerning Ref. [21]. MGA thanks the LANL T-2 Group for its hospitality and support during the completion of this work. VC and MG acknowledge support by the DOE Office of Science and the LDRD program at Los Alamos National Laboratory. MGA was supported by the U.S. DOE contract DE-FG02-08ER41531 and by the Wisconsin Alumni Research Foundation.

## References

- [1] S. Weinberg, J.Phys.Conf.Ser. **196**, 012002 (2009).
- [2] N. Severijns, M. Beck, and O. Naviliat-Cuncic, Rev. Mod. Phys. **78**, 991 (2006), nucl-ex/0605029.
- [3] P. Herczeg, Prog. Part. Nucl. Phys. **46**, 413 (2001).
- [4] S. Profumo, M. J. Ramsey-Musolf, and S. Tulin, Phys.Rev. **D75**, 075017 (2007), hep-ph/0608064.



- [5] S. Bauman, J. Erler, and M. Ramsey-Musolf, (2012), 1204.0035.
- [6] T. Lee and C.-N. Yang, Phys.Rev. **104**, 254 (1956).
- [7] J. D. Jackson, S. B. Treiman, and H. W. Wyld, Phys. Rev. **106**, 517 (1957).
- [8] T. Bhattacharya *et al.*, Phys.Rev. **D85**, 054512 (2012), 1110.6448.
- [9] Particle Data Group, K. Nakamura *et al.*, J.Phys.G **G37**, 075021 (2010).
- [10] J. Green *et al.*, (2012), 1206.4527.
- [11] V. Cirigliano, J. Jenkins, and M. Gonzalez-Alonso, Nucl.Phys. **B830**, 95 (2010), 0908.1754.
- [12] CKMfitter Group, J. Charles *et al.*, Eur. Phys. J. **C41**, 1 (2005), hep-ph/0406184.
- [13] V. Mateu and J. Portoles, Eur.Phys.J. **C52**, 325 (2007), 0706.1039.
- [14] D. Britton *et al.*, Phys.Rev.Lett. **68**, 3000 (1992).
- [15] G. Czapek *et al.*, Phys.Rev.Lett. **70**, 17 (1993).
- [16] V. Cirigliano and I. Rosell, Phys.Rev.Lett. **99**, 231801 (2007), 0707.3439.
- [17] J. Hardy and I. Towner, Phys.Rev. **C79**, 055502 (2009), 0812.1202.
- [18] M. Bychkov *et al.*, Phys.Rev.Lett. **103**, 051802 (2009), 0804.1815.
- [19] M. Voloshin, Phys.Lett. **B283**, 120 (1992).
- [20] P. Herczeg, Phys.Rev. **D49**, 247 (1994).
- [21] B. A. Campbell and D. W. Maybury, Nucl.Phys. **B709**, 419 (2005), hep-ph/0303046.
- [22] W. Wilburn *et al.*, Rev. Mex. Fis. **Suppl. 55**, 119 (2009).
- [23] R. Alarcon *et al.*, Precise Measurement of Neutron Decay Parameters, 2007.
- [24] Nab Collaboration, D. Pocanic *et al.*, Nucl.Instrum.Meth. **A611**, 211 (2009), 0810.0251.
- [25] K. P. Hickerson, The Fierz Interference Term in Beta-Decay Spectrum of UCN, 2009, UCN Workshop, November 6–7 2009, Santa Fe, New Mexico.
- [26] A. Knecht *et al.*, Nucl.Instrum.Meth. **A660**, 43 (2011).
- [27] J. D. Jackson, S. B. Treiman, and H. W. Wyld, Nuclear Physics **4**, 206 (1957).
- [28] V. D. Barger, A. D. Martin, and R. Phillips, Z.Phys. **C21**, 99 (1983).

- [29] J. Pumplin *et al.*, JHEP **0207**, 012 (2002), hep-ph/0201195.
- [30] CMS Collaboration, S. Chatrchyan *et al.*, JHEP **1208**, 023 (2012), 1204.4764.
- [31] A. D. Martin, W. J. Stirling, R. S. Thorne, and G. Watt, Eur. Phys. J. **C63**, 189 (2009), 0901.0002.
- [32] ATLAS Collaboration, G. Aad *et al.*, (2012), 1209.4446.
- [33] CMS Collaboration, Search for leptonic decays of W' bosons in pp collisions at  $\sqrt{s}=8$  TeV, CMS-PAS-EXO-12-010.
- [34] D. J. Broadhurst and A. Grozin, Phys.Rev. **D52**, 4082 (1995), hep-ph/9410240.
- [35] CMS Collaboration, S. Chatrchyan *et al.*, (2012), 1206.1849.
- [36] T. Sjostrand, S. Mrenna, and P. Z. Skands, JHEP **0605**, 026 (2006), hep-ph/0603175.
- [37] T. Sjostrand, S. Mrenna, and P. Z. Skands, Comput.Phys.Commun. **178**, 852 (2008), 0710.3820.